

# QE Overestimation and Deterministic Crosstalk Resulting from Inter-pixel Capacitance

Andrew C. Moore\*  
*RIT*

Zoran Ninkov†  
*RIT*

Bill Forrest‡  
*UR*

Pixels in both hybridized and monolithic CMOS detector arrays may couple capacitively to their neighboring pixels — this “inter-pixel capacitance” can significantly distort the characterization of conversion efficiency and MTF in CMOS devices. These effects have been largely unaccounted for in measurements to date. In this paper, the effects of this coupling are investigated. Compensation methods for these errors are described and applied to silicon P-I-N array measurements. The measurement of Poisson noise, traditionally done by finding the mean square difference in a pair of images, needs to be modified to include the mean square correlation of differences with neighboring pixels.

## I. INTRODUCTION

CMOS detector arrays operate in a “non-destructive” readout mode that measures the voltage produced by a detector node (pixel) without transferring it out of the pixel. In such arrays, small amounts of stray capacitance can couple pixels to neighboring pixels and influence the voltage read for that pixel. This coupling is inter-pixel capacitance. Inter-pixel capacitance can be very prominent in deeply or fully depleted (P-I-N) detectors, partly due to the higher dielectric constant of the detector substrate and partly due to the low detector capacitance that comes with deep or full depletion.

Inter-pixel capacitance creates two effects. The first and most obvious is that crosstalk is generated — a strong signal in one pixel creates a weak signal in neighboring pixels. This observed crosstalk may easily be mistaken for a more common crosstalk — diffusion crosstalk — which occurs when photocarriers generated within one pixel diffuse to adjacent pixels. A second effect naturally exists as well. The signal appearing in those neighboring pixels is signal that “should have” appeared in the central pixel had there been no inter-pixel capacitance. The signal in the central pixel is therefore attenuated. This attenuation may also be mistaken for attenuation resulting from diffusion.

Crosstalk from diffusion and crosstalk from capacitive coupling are the result of different mechanisms and have different properties. Crosstalk from diffusion occurs before charge collection and is stochastic — Poisson noise from diffusion crosstalk is completely uncorrelated in neighboring pixels. Crosstalk from inter-pixel capacitance occurs after charge collection and is deterministic — Poisson noise observed with inter-pixel capacitive crosstalk is correlated in neighboring pixels. Given a choice between the two mechanisms, crosstalk from inter-pixel coupling is more desirable.

The presence of inter-pixel capacitance in detector arrays was anticipated in simulations performed by Kavadias *et al.* circa 1993.<sup>1</sup> Caccia *et al.*<sup>2,3</sup> measured inter-pixel coupling in a hybrid “Vertex” detector for a supercollider in 2000. Moore *et al.*<sup>4</sup> first suggested that inter-pixel capacitance can create significant errors in the “noise-squared versus signal”<sup>5,6</sup> method of estimating conversion factor (quanta per output unit, such as electrons per microvolt), and presented data supporting this suggestion. The effects of inter-pixel capacitance and the mechanisms which cause them were investigated in more detail in a second paper.<sup>7</sup>

Inter-pixel capacitance causes Poisson noise in a device to be attenuated. As a result, the responsive quantum efficiency (RQE) is *overestimated* — the detector array appears to be collecting more photons than it actually is. Capacitive crosstalk of 1% to each neighboring pixel will attenuate noise amplitude by 4% and result in an 8% error in the measurement of noise power (variance) and thus in noise-squared versus signal — resulting in at least 8% more observing time to achieve the expected signal to noise ratio.

For scientific detector arrays in low-signal applications such as space telescopes, the RQE of the array is the “bottom line” as to its information-gathering ability — arrays with poorer RQE take longer to accumulate the same information, and are proportionally that much more “expensive” (in observing time) to operate in order to make the same scientific discoveries. Since relatively small amounts of interpixel capacitance can create large errors in the measurement of RQE, even small amounts of crosstalk (observable in the vicinity of either hot pixels or cosmic events) may be a warning sign that actual RQE is *significantly lower* than reported RQE determined using “noise squared versus signal” methods.

Inter-pixel capacitance is expected to become more significant with modern arrays. As detector array designers

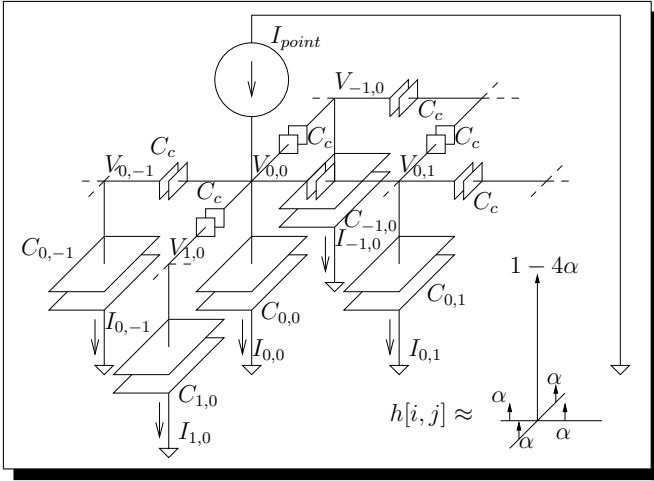


Figure 1: Photocurrent physically entering a detector node may leave the node as displacement current through small coupling capacitors (labeled  $C_c$ ) and appear on adjacent nodes instead. Even if all quanta are captured by the central  $C_{0,0}$ , signal still appears on neighboring nodes that have captured no quanta.

continue to strive for the simultaneous qualities of high pixel density (requiring small distances between pixel centers) high quantum efficiency, low diffusion crosstalk, and low latent images (requiring 100% fill factor — small gaps between pixel implants) and high sensitivity (low capacitance multiplexer nodes) the stray capacitance to neighboring pixels will be more pronounced. Stray capacitance to a detector node is the result of the presence of conductors adjacent to the detector node. Detector nodes *must* be conductive to accumulate charge. Thus, the nearest conductors adjacent to the pixels in the lowest capacitance detector arrays will be the neighboring pixels.

## II. BASIC MECHANISM

A photo-detector array is modeled here as an array of capacitors  $C[i, j]$ , each receiving a signal  $Q[i, j]$  that is the accumulated photo-current *entering* node  $i, j$  over some integration time  $\Delta t$ . We consider input signals that do not change over time, so

$$Q[i, j] = \int_t^{t+\Delta t} I[i, j](\tau) d\tau \approx I[i, j] \Delta t. \quad (1)$$

All capacitors  $C[i, j]$  are assumed equal by fabrication so  $C[i, j] = C_{node}$ . The array is modeled as a discrete linear shift-invariant<sup>8</sup> (LSI) system, outputting an array of voltages:

$$V[i, j] = \sum_{m=-\infty}^{\infty} \sum_{n=-\infty}^{\infty} Q[i, j] h_c[i - m, j - n]. \quad (2)$$

or, more simply:

$$V[i, j] = Q[i, j] * h_c[i, j]. \quad (3)$$

where  $*$  is the 2D convolution operator and  $h_c[i, j]$  is the impulse response of the collection array.

Ideally,

$$h_c[i, j] = \frac{\delta[i, j]}{C_{node}}. \quad (4)$$

where  $\delta[i, j]$  is the discrete 2D “unit impulse” or “delta function”. The ideal output of the array is simply a voltage  $V[i, j]$  such that

$$V[i, j] = \frac{Q[i, j]}{C_{node}}. \quad (5)$$

Equation 5, although very simple, has been the nodal electrical model to date. Inter-pixel capacitance introduces a new “electrical crosstalk” mechanism.

Upon introducing small coupling capacitors  $C_c$  between detector nodes (pixels on the array) as shown in Figure 1, photo-current into a single detector node returns via multiple paths. From Kirchoff’s current law, the total charge entering the node (at the top of Figure 1) is equal to the total charge appearing electrically on that node and its neighbors:

$$Q_{point} = I_{point} \Delta t = \sum_{i,j} I_{i,j} \Delta t = \sum_{i,j} A[i, j]. \quad (6)$$

where  $I_{i,j}$  is the current through  $C[i, j]$  and  $A[i, j]$  is the *apparent* charge appearing electrically on that node.

Thus,

$$\sum_{i,j} V[i, j] = \sum_{i,j} \frac{A[i, j]}{C_{node}} = \frac{Q_{point}}{C_{node}}. \quad (7)$$

and the photo-carriers collected in a single node appear upon readout to be distributed into several nodes, but only the nodal capacitance  $C_{node}$  appears in the “DC” output of the detector array. The impulse response of the detector nodes is

$$h_c[i, j] = \frac{A[i, j]}{Q_{point} C_{node}}. \quad (8)$$

At this point, we normalize out the nodal capacitance  $C_{node}$  and express the impulse response as a deviation from ideal response — the ratio of apparent charge  $A$  to actual collected charge  $Q$ . Thus,

$$h[i, j] = h_c[i, j] C_{node} = \frac{A[i, j]}{Q_{point}}. \quad (9)$$

and

$$\sum_{i,j} h[i, j] = 1. \quad (10)$$

Since inter-pixel capacitance pulls the voltages of neighboring nodes in the same direction,

$$h[i, j] \geq 0. \quad (11)$$

Also, the circuit is passive and cannot create an output greater than its input. Thus:

$$h[i, j] \leq 1. \quad (12)$$

Symmetry is a direct consequence of the array of identical pixels. We do not assume that vertical coupling is equal to horizontal coupling, or that the diagonal couplings are equal, but simply that a pixel will couple to a neighbor the same way that neighbor will couple back to it.

$$h[i, j] = h[-i, -j]. \quad (13)$$

Photo-current arrives in detector nodes quantized by the charge of an electron. Photon arrival and diffusion in the detector are both stochastic processes, and without correlation mechanisms in photon arrival, carrier generation and diffusion, the individual collection events are statistically independent and obey Poisson statistics. Thus, charge collected by detector nodes may be expressed as a mean signal component  $M[i, j]$  plus a “white” noise image  $N[i, j]$

$$Q[i, j] = M[i, j] + N[i, j]. \quad (14)$$

The white noise image has a uniform power spectral density  $S_N$ —

$$\begin{aligned} S_N(\xi, \eta) &= \lim_{T \rightarrow \infty} \frac{E \left\{ \left| \mathcal{F} \{ N[i, j] \} \right|^2 \right\}}{2T} \\ &= \lim_{T \rightarrow \infty} \frac{E \left\{ |F_N(\xi, \eta)|^2 \right\}}{2T} \\ &= \sigma_N^2. \end{aligned} \quad (15)$$

where  $E\{\}$  is the expectation operator,  $\mathcal{F}\{\}$  is the Fourier transform operator resulting in  $F_N(\xi, \eta)$ , and  $\xi$  and  $\eta$  are spatial frequency (in  $x$  and  $y$ ) expressed in cycles per pixel. The inter-pixel capacitive impulse response  $h[i, j]$  causes apparent charge to be a spatially filtered version of the actual charge. The observed output is:

$$A[i, j] = (M[i, j] + N[i, j]) * h[i, j]. \quad (16)$$

In the absence of an internal gain mechanism in the detector itself, i.e., assuming one electron per photon, the variance of the noise image is equal (in quanta) to the mean signal  $M$ :

$$\sigma_M^2[i, j] = M[i, j]. \quad (17)$$

The difference  $D[i, j]$  of a pair of otherwise identically acquired images  $A_1$  and  $A_2$  cancels out the signal component and leaves a noise image that is twice the variance of the original images’ noise components.

$$D[i, j] = A_1[i, j] - A_2[i, j] = (N_1[i, j] - N_2[i, j]) * h[i, j]. \quad (18)$$

The noise energy in this difference image is typically compared to the mean of the sum of the images to obtain an estimate of the conversion factor. Uniform illumination  $M[i, j] = M$  is typically used, but is not required and has not been assumed. Assuming the noise difference image is stationary, (this covers random spatial variations in illumination and detector efficiency) the power spectral density of the noise image in Equation 18 is

$$S_D(\xi, \eta) = 2\sigma_N^2 |H(\xi, \eta)|^2. \quad (19)$$

Thus, the power spectral density of the observed difference image yields information about the inter-pixel capacitive effect. Since the input signal (the noise on the charge collected by the nodes) is white (a constant) the output power spectrum is proportional to the squared magnitude of the Fourier transform of the impulse response.

Direct measurement of the power spectra of random processes by averaging spectra from samples is generally discouraged; autocorrelation techniques are preferred. The Weiner-Khinchine relation in two dimensions

$$S(\xi, \eta) = \sum_{x, y} R[x, y] e^{-j2\pi\xi x} e^{-j2\pi\eta y} = \mathcal{F} \{ R[x, y] \}. \quad (20)$$

expresses the power spectral density of a 2D random process in terms of its autocorrelation function. The power spectral density of a 2D stationary random process  $S(\xi, \eta)$  is obtained by measuring its autocorrelation function  $R[x, y]$ , then taking the Fourier transform of that.

Combining Equations 19 and 20 results in:

$$\mathcal{F} \{ R_D[x, y] \} = 2\sigma_N^2 |H(\xi, \eta)|^2 = 2\sigma_N^2 H(\xi, \eta) H^*(\xi, \eta). \quad (21)$$

or, equivalently:

$$\mathcal{F} \{ R_D[x, y] \} = 2\sigma_N^2 \mathcal{F} \{ h[x, y] * h[-x, -y] \}. \quad (22)$$

Taking the inverse Fourier transform of Equation 22 yields

$$R_D[x, y] = 2\sigma_N^2 h[x, y] * h[-x, -y]. \quad (23)$$

The output autocorrelation is equal to the correlation of the impulse response with itself, scaled by the Poisson noise power at the input.

Since the impulse response  $h[i, j]$  has unit area, its correlation with itself does also, and the summation of Equation 23 results in:

$$\sum_{i, j} R_D[i, j] = 2\sigma_N^2. \quad (24)$$

**Equation 24 is the key result**, and should be used to estimate “noise squared” in lieu of the traditionally applied variance estimator

$$\widehat{R}_D [0, 0] = \widehat{2\sigma_N^2} = \widehat{D^2} = \frac{\sum_{i,j} D^2 [i, j]}{N}. \quad (25)$$

which does not account for inter-pixel coupling.

Since (Equations 11 and 13)  $h[x, y]$  is non-negative and even, no phase information is actually removed by the magnitude operator and another expression for Equation 22 is:

$$\frac{\mathcal{F}\{R_D[x, y]\}}{2\sigma_N^2} = (\mathcal{F}\{h[x, y]\})^2. \quad (26)$$

Taking the square root of Equation 26 first (this can also be done here since  $h[x, y]$  and  $H(\xi, \eta)$  are both non-negative and even) and then taking the inverse Fourier transform results in

$$\mathcal{F}^{-1} \left\{ \left[ \frac{\mathcal{F}\{R_D[x, y]\}}{2\sigma_N^2} \right]^{\frac{1}{2}} \right\} = h[x, y]. \quad (27)$$

This is a direct expression which may be used to obtain the impulse response of inter-pixel capacitance from the autocorrelation of the shot noise in a difference image.

The total power of the output power spectral density in Equation 19 is the mean square output, and by Parseval’s relation, is:

$$\begin{aligned} \overline{D^2} &= R_D [0, 0] \\ &= 2\sigma_N^2 \int \int |H(\xi, \eta)|^2 d\eta d\xi \\ &= 2\sigma_N^2 \sum_{i,j} h^2 [i, j]. \end{aligned} \quad (28)$$

Thus, the sum of the squares of the impulse response is the attenuation of the white input noise variance caused by the inter-pixel capacitance. From Equations 10, 11, and 12, this is indeed attenuation — always less than one if there is any coupling.

### III. MEASUREMENT OF COUPLING BY AUTOCORRELATION

Lifting the correlation out of the noise images takes substantial averaging. For a uniform strength of  $\mu$  quanta, the variance of the incoming Poisson noise is  $\mu$  quanta squared. We assume here that  $\mu$  is large enough that a Gaussian approximation is appropriate. A difference image will have a variance  $2\mu$  quanta squared of noise, but zero mean. The variance of the product of any uncorrelated pair  $x, y$  of these noise values is equal to:

$$\begin{aligned} \mathbb{E} [(xy)^2] &= \mathbb{E} [x^2 y^2] \\ &= \mathbb{E} [x^2] \mathbb{E} [y^2] \\ &= 4\mu^2. \end{aligned} \quad (29)$$

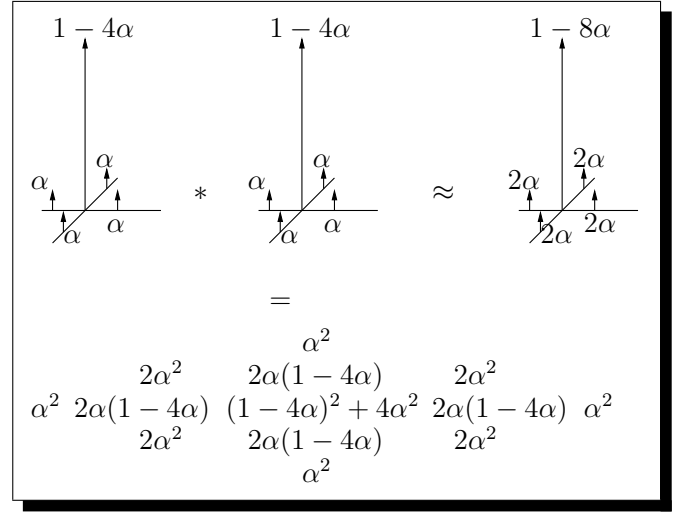


Figure 2: The autocorrelation of the 2d impulse response is equal to the expected correlation coefficients  $R$ . Neglecting the tiny  $\alpha^2$  terms results in nearest-neighbor correlation coefficients of  $2\alpha$ , leaving  $1 - 8\alpha$  in the center.

which is a variance (in quanta to the fourth power) that is the square of the mean variance in the difference image itself.

If the pair  $x, y$  is completely correlated, this variance is doubled.

$$\begin{aligned} \mathbb{E} [(x^2)^2] - \mathbb{E}^2 [x^2] &= \mathbb{E} [x^4] - 4\mu^2 \\ &= 3\mathbb{E}^2 [x^2] - 4\mu^2 \\ &= 8\mu^2. \end{aligned} \quad (30)$$

If accurately measured cross-correlation of some fraction  $\alpha$  of the photon noise is desired, we require that  $N$  averages are performed such that the standard deviation of the cross-correlation estimator is less than some small fraction of the mean square pixel noise in a difference image:

$$\frac{2\mu}{\sqrt{N}} \ll \alpha 2\mu. \quad (31)$$

Dropping the dependency on the signal strength and rearranging yields:

$$N \gg \frac{1}{\alpha^2}. \quad (32)$$

So, bringing a one percent correlation signal up to the noise level requires averaging 10000 samples. Raising it a factor of ten above the noise requires a million samples.

In most cases, only correlation to the immediate neighbors needs to be considered — for small but significant amounts of inter-pixel coupling, the “second neighbor” coupling may be considered effectively zero. It should be

apparent from inspection of the autocorrelation if more terms are required. Neglecting “second neighbor” and “diagonal neighbor” coupling, the center node loses  $4\alpha$  of its charge —  $1\alpha$  to each of its four nearest neighbors — so the impulse response is approximated by

$$\begin{aligned} h[i, j] = & (1 - 4\alpha) \delta[i, j] \\ & + \alpha\delta[i + 1, j] + \alpha\delta[i - 1, j] \\ & + \alpha\delta[i, j + 1] + \alpha\delta[i, j - 1]. \end{aligned} \quad (33)$$

and the resulting convolution is shown in Figure 2.

The center term of the convolution,  $R[0, 0]/2\sigma_N^2 = \overline{h^2} \approx (1 - 4\alpha)^2 \approx 1 - 8\alpha$ , also expressed in Equation 28, is the relative mean square output of the noise compared to what would be measured without any inter-pixel coupling — the factor by which conversion gain is in error when inter-pixel capacitance is significant. The approximation  $1 - 8\alpha$  holds for small amounts of coupling, and illustrates the magnitude of error this effect can cause. 1% coupling to each of four neighbors can cause a 8% error in estimated conversion factor.

Assuming most inter-pixel coupling is to these four immediate neighbors, a simple algorithm for estimating Poisson noise  $\sigma_D^2$  in a scene, given  $D$ , the difference of two acquisition instances of the scene, is

$$\begin{aligned} \widehat{\sigma_D^2} = & \frac{1}{2N} \left[ \sum_{i,j} D^2[i, j] \right. \\ & + 2 \sum_{i,j} D[i, j] D[i + 1, j] \\ & \left. + 2 \sum_{i,j} D[i, j] D[i, j + 1] \right]. \end{aligned} \quad (34)$$

where  $N$  is the number of pixels. The second and third terms in Equation 34 are doubled because the center pixel has two horizontal and two vertical neighbors. The overall result is divided by  $2N$  because the variance in the difference image is twice the variance of the original image. This estimator of Poisson noise may be used in the “slope of noise variance versus signal” method of estimating conversion factor described by Mortara and Fowler<sup>5</sup>.

#### IV. MECHANISMS OF INTER-PIXEL COUPLING

In our first paper<sup>4</sup>, we suggested the coupling was between the parallel faces of the indium bumps. This hypothesis was incorrect. Analysis and simulation<sup>7</sup> indicated that coupling exists mainly through fringing fields between the edges of the pixel implants.

Two different types of detector are considered here which couple pixel-to-pixel with two different field paths.

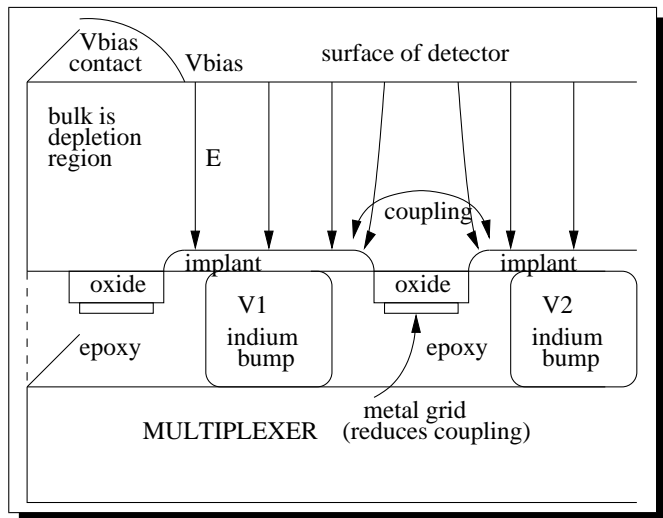


Figure 3: Some coupling in fully depleted detectors occurs in the detector bulk. In silicon, this is enhanced by a relatively high dielectric constant. The metal grid in the PIN detector tested inhibited additional coupling underneath the detector.

The first is a hybridized silicon PIN array for visible imaging — a detector with fully depleted bulk. The second is a hybridized indium antimonide array for infrared imaging, a “per-pixel” depleted detector.

The hybridized silicon PIN array, shown in Figure 3, is somewhat unusual — with the detector bulk fully depleted, electric fields exist throughout. A metal grid, deposited on thick oxide between the pixels, controls the electrical state of the silicon gap between the pixel implants. This voltage is biased to keep the inter-pixel gap out of inversion and accumulation. The presence of this grid also (unintentionally) prevents significant inter-pixel coupling in the space between the indium bumps — it heavily influences the potential in this region where significant coupling otherwise would occur. It must do this, unfortunately, by increasing the nodal capacitance, and thus reducing sensitivity.

A hybridized indium antimonide array, depicted in Figure 4 is a more typical detector. The bulk is doped opposite that of the implants, and each pixel maintains a separate depletion region close to the pixel implant. The bulk of the detector, however, is conductive. No electric field, and therefore no inter-pixel capacitive coupling, can exist in the detector bulk. There is no metal grid controlling the surface state in the gaps between pixels in the illustration however (although some per-pixel depleted arrays do have field control grids.)

The gaps between the pixels in a per-pixel depleted detector are conductive, and should shield neighboring pixels from each other somewhat, but not completely. Since the gap varies with pixel bias, this predicts that inter-pixel coupling in per-pixel depleted devices is non-linear, and that it decreases as the nodes collect photocarriers.

There is, of course, no reason necessitating undepleted gaps between pixels; detector arrays fall in between these

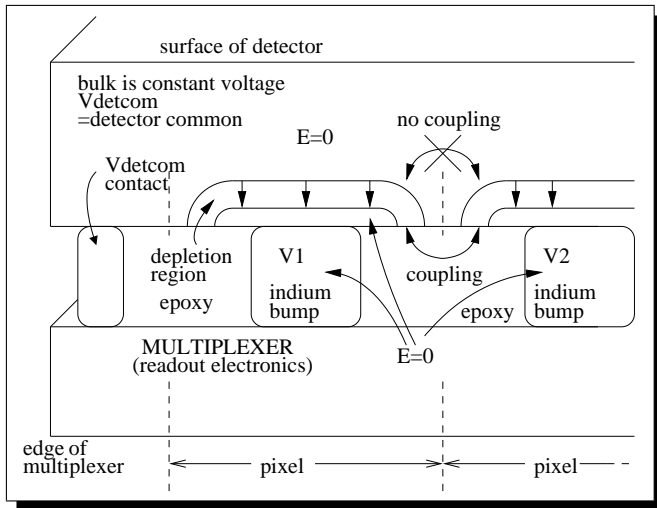


Figure 4: Coupling in a more typical per-pixel depleted detector occurs in the space between the readout and the detector. Fully-biased detectors have a smaller gap between depletion regions, and should exhibit non-linear interpixel coupling that decreases as the pixels accumulate charge and the inter-pixel gap widens.

-574	16196	23060	5123	521
9578	63021	253064	61183	12483
30770	258440	4044351	259273	30120
12989	59031	252469	64626	11585
-83	5127	21765	16001	468

Table I: Observed P-I-N noise correlation indicates a nearest neighbor correlation of 6 percent of the central value, and thus a 3 percent coupling, agreeing with other observations.

two extremes. Full depletion of these gaps does not create a short between adjacent pixels — if it did, P-I-N devices would not work. However, most CMOS detector arrays cannot tolerate the deep depletion shown in Figure 3 and CMOS depletion regions tend to be smaller and closer to the implant<sup>9</sup>.

## V. AUTOCORRELATION OBSERVED IN P-I-N AND INSB ARRAYS

Table I shows a typical observed autocorrelation of observed Poisson noise from many difference images taken with a prototype silicon P-I-N array made by Raytheon.

These values were computed by analyzing the autocorrelation in hundreds of patches taken from approximately one hundred difference images. Autocorrelation of many 50 by 50 patches was computed as the sum of the product of the pixels in the difference image divided by the number of pixels in the patch. Patches were rejected if they appeared to be tainted by a cosmic event. Typically, several hundred to several thousand patches were used,

296	-441	-927	-1170	-242
-1186	1499	14341	2357	-482
-187	15236	476374	15200	145
-140	2609	14502	1173	-1015
-191	-1373	-1295	-296	734

Table II: Observed InSb noise correlation indicates 3 percent correlation, or 1.5 percent coupling — a somewhat questionable result.

each with 2500 samples (pixels), representing a sample size on the order of a million, satisfying Equation 32.

The averaging strategy used in Table I resulted in a calculated uncertainty of roughly 4000 units, as computed from Equation 29. It can be seen that the outermost values are indeed within 4000 of the expected zero correlation, but the nearest neighbors, the nearest diagonal neighbors, and even the second horizontal neighbors exhibit mean correlations sums that are at least 5 to ten standard deviations away from this expected zero. We can quite confidently assert that this observed noise is not Poisson distributed.

The nearest-neighbor correlation is 255 thousand, roughly 6.3 percent of the central value of 4.04 million. This percentage is twice the coupling (see Figure 2) and thus indicates coupling of  $\alpha = 3.1$  percent. This small amount of coupling (*i.e.*, the coupling capacitor is 3.1 percent of the nodal capacitor, as shown in Figure 1) resulted in an initial overestimation of P-I-N conversion factor by roughly 31 percent — a very large error — large enough that the  $8\alpha$  approximation is not holding very well.

We also note that, by Equation 13, left-neighbor and right-neighbor correlation coefficients should be identical — as should the up and down neighbor coefficients. The slight differences seen in these data are the result of a simple correlation algorithm effectively applied to only slightly different data sets. A more efficient algorithm would measure horizontal and vertical correlations once, and use the same estimator for both directions of coupling.

The correlation data in Table II were obtained from similar tests performed on an InSb array at the University of Rochester's Near Infrared Astronomy Lab. Very long wavelengths produced too strong of a signal to attenuate read noise with Fowler sampling, so near-visible wavelengths were used.

These data indicate a 1.5 percent coupling to adjacent pixels in the InSb arrays — a result that seems high when compared to tests using hot pixels. (Hot pixels indicated only 0.5 percent coupling) Several effects may have caused the discrepancy. First, a small amount of photoconductive gain may have been present in this (longer wavelength) device, resulting in additional correlation. Second, the hot pixels were fully depleted, resulting in a larger inter-pixel gap. The autocorrelation tests

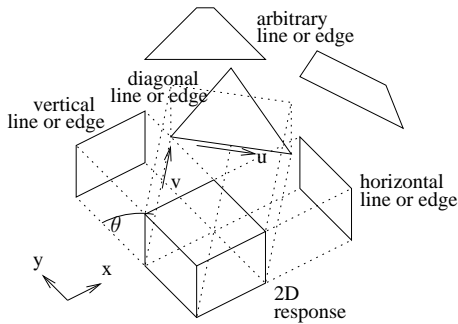


Figure 5: For edge spread modeling, the projection of the pixel is required. For vertical and horizontal projections, a square pixel appears to be box shaped. A 45 degree projection yields a triangular shape. At arbitrary angles, a square pixel has a trapezoidal projection.

were performed with small amounts of signal, and the nearly fully biased pixels had a smaller inter-pixel gap that should have yielded more coupling. We conclude that coupling is present, but we are yet uncertain of its exact magnitude and/or dependence upon detector bias.

## VI. EDGE SPREAD AND INTER-PIXEL CAPACITANCE

In the silicon P-I-N arrays, inter-pixel coupling was significant enough to influence the observed edge spread. The edge spread function, or ESF, is the integral of the line spread function, or LSF — which itself is the convolution of a line impulse with the point spread function, or PSF. For circularly symmetrical PSF such as that produced by diffusion in an array of continuous pixels, the Abel transform derives a unique LSF from the PSF<sup>8</sup>. P-I-N devices should produce Gaussian PSF from diffusion, and the Abel transform of Gaussian PSF yields Gaussian LSF and an “error function” shaped edge spread.

Pixels are not circularly symmetrical and are typically in a square grid. The overall response is more properly characterized by a pixel response function (or PRF) that may be directly obtained by spot-scanning<sup>10</sup> techniques. This PRF yields line spread (pixel projection) and resulting edge spread that varies with angle. Here, we assume a square PRF. We use the variable  $u$  to represent distance from some central location along some projection at an angle  $\theta$ . At arbitrary angles, the projection of a square pixel (shown in Figure 5) can be represented as the convolution of a pair of rect (or “boxcar”) functions — each of unit area but with a width proportional the cosine or sine of the angle.

$$\text{pixel}_\theta(u) = \frac{\text{rect}(u \sin(\theta))}{\sin(\theta)} * \frac{\text{rect}(u \cos(\theta))}{\cos(\theta)}. \quad (35)$$

At zero and 90 degrees, one of the rect functions has zero width — it is an impulse function. At 45 degrees the

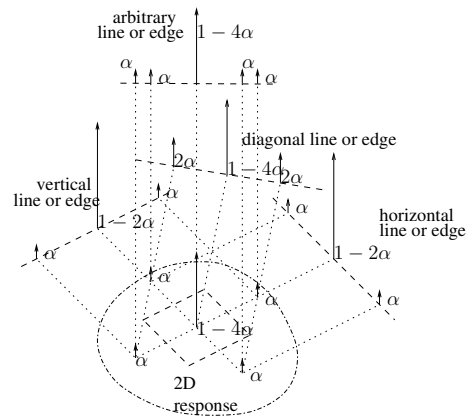


Figure 6: The center pixel and four nearest neighbors in the inter-pixel response appear at different relative positions as a function of angle, but their intensities do not change. At zero, 45 and 90 degrees, some pixels coincide and their responses add together.

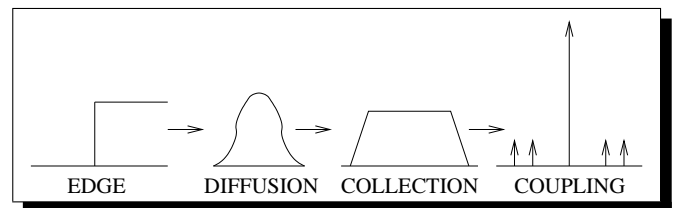


Figure 7: Expected edge spread is the convolution of the optical edge, the diffusion profile, the pixel collection profile, and the interpixel capacitance profile.

rect functions are identical and a triangle shaped function results.

The four nearest neighbor pixels contribute via inter-pixel coupling, as shown in Figure 6, resulting in a 1D projection of the 2D impulse response in Equation 33 at angle  $\theta$ :

$$\begin{aligned} \text{ipcap}_\theta(u) = & \alpha[\delta(u + \sin(\theta)) + \delta(u - \sin(\theta)) \\ & + \delta(u + \cos(\theta)) + \delta(u - \cos(\theta))] \\ & + (1 - 4\alpha)\delta(u). \end{aligned} \quad (36)$$

The expected edge spread is the convolution of the diffused edge (an integrated Gaussian) with Equations 35 and 36, as illustrated in Figure 7.

$$\text{ESF}_\theta(u) = \text{pixel}_\theta(u) * \text{ipcap}_\theta(u) * \int_{-\infty}^u \frac{\text{Gaus}(\sigma b)}{b} d\sigma. \quad (37)$$

We produced optically sharp edges at varying angles on the P-I-N arrays<sup>4</sup>, and processing of many resulting images repeatably produced the edge profile shown in Figure 8. This particular edge was horizontal. Only by including inter-pixel coupling in the model could we

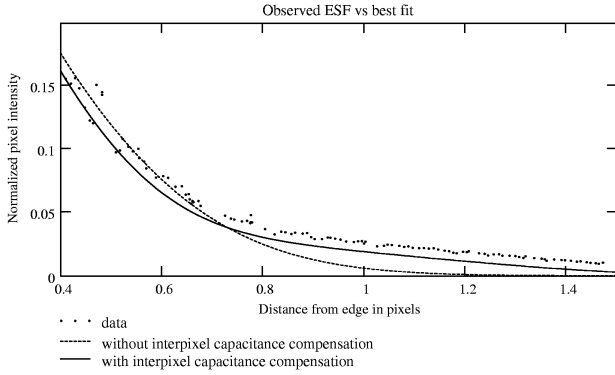


Figure 8: A closeup of observed and expected edge spread compared with the best-fit Gaussian-only model. Inter-pixel coupling correctly predicts the shape of the edge spread in the pixel adjacent to the center of the edge.

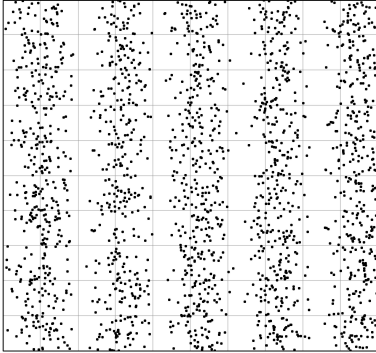


Figure 9: A stochastically generated sine wave illustrates the signal and noise at high spatial frequencies associated with low photon fluxes.

find agreement between expected and actual results. The best-fit edge from a model that only included Gaussian carrier diffusion is included in the figure for comparison.

Edge response at 45 degrees was also modeled, and a slight difference between diagonal edges and vertical or horizontal edges was expected. We were able to observe these slight differences as well, but the results just verify the 2D edge spread model and don't shed much additional illumination on interpixel capacitance — and thus are not included here.

## VII. INTER-PIXEL CAPACITANCE AND DQE

The true measure of a detector array's performance is its detective quantum efficiency, or DQE. DQE, the squared SNR at the output of the array compared to the squared SNR incident at the surface of the array, is a power ratio. It tells how much power is necessary in an imperfect detector to attain the SNR that a perfect detector would get. Zero-frequency DQE may depend upon

other conditions, such as signal and background levels and exposure time. We neglect background levels here and just consider the additional DQE loss that occurs at high spatial frequencies, as pioneered by Doerner,<sup>11</sup> and built upon by Shaw<sup>12</sup>, Van Metter, Rabbani<sup>13,14</sup>, Yao and Cunningham<sup>15</sup>, and others. Doerner generalized the definition of DQE for imaging application to include a spatial frequency dependence. Figure 9 shows a stochastically generated two dimensional sine wave that may help visualize the signal and noise at high spatial frequencies. Stochastic scattering from diffusion reduces DQE at high spatial frequencies, and in an otherwise perfect detector, DQE is reduced by the square of  $T(\xi)$ , the scattering MTF<sup>13,14</sup>:

$$DQE(\xi) = |T(\xi)|^2. \quad (38)$$

In fully depleted arrays such as the Si PIN device shown in Figure 3, stochastic scattering leads to a Gaussian scattering MTF. In detectors with “per-pixel” depletion regions as shown in Figure 4, such as the InSb devices, the MTF is approximately<sup>16,17</sup>:

$$T(\xi) = \frac{2e^{-2\pi\xi}}{1 + e^{-4\pi\xi}}. \quad (39)$$

where  $\xi$  is the spatial frequency in cycles per detector thickness. (Thinner detectors have better MTF.)

Inter-pixel capacitance, like scattering, also reduces MTF. This response is easily derived from the inter-pixel coupling impulse response given in Equation 33 and the shifting property of the Fourier transform, yielding:

$$T(\xi, \eta) = (1 - 2\alpha + 2\alpha \cos(2\pi\xi)) \cdot (1 - 2\alpha + 2\alpha \cos(2\pi\eta)). \quad (40)$$

for small  $\alpha$ . In Equation 40,  $\xi$  and  $\eta$  are spatial frequency in cycles per pixel — the minimum MTF is at the Nyquist frequency of one cycle per two pixels.

It is very easy to mistakenly attribute the effects of inter-pixel capacitive coupling to diffusion. Inter-pixel capacitance is a deterministic scattering mechanism however, and **attenuates photon noise and signal identically at all spatial frequencies**. Diffusion would cause some of the carriers shown in Figure 9 to wander to neighboring pixels, and information about their origin would become more uncertain. Inter-pixel coupling does not cause such a loss of information. Thus, inter-pixel capacitance has no effect upon *device* DQE, and its effect should be distinguished from diffusion MTF for the purpose of accurately evaluating expected  $DQE(\xi, \eta)$  for an array.

The inter-pixel capacitive effect *can* cause errors in the *measurement* of DQE, as it reduces the observed Poisson noise and causes DQE to be overestimated the same way RQE is overestimated. DQE is commonly measured by illuminating an array with a known photon flux (thus a known input SNR) and measuring the SNR observed at the array output. Since the observed noise is attenuated by interpixel coupling but the observed signal is

unaffected, such measurements can inexplicably indicate DQE exceeding 100 percent.

### A. Assumptions and Simplifications used here

This analysis has used several simplifications, but none that seem significant. First, pixels are frequently non-linear — the capacitance changes with voltage. This non-linearity can be ignored if the stochastic signal considered (the Poisson noise) is small compared to the well depth of the pixel. Pixel non-linearity can also cause significant error in measurement of conversion factor.<sup>18</sup>

There are also slight variations in nodal capacitance that were ignored here. There is strong evidence that inter-pixel capacitive coupling is not symmetrical around defective (“hot”) pixels in InSb arrays. Normal pixels are likely have slight variations as well, but the average coupling must be symmetrical. Should a complete map of pixel capacitance, including coupling, be desired, it should be obtainable from a very large number of noise images — as given by Equation 32.

Our pixel response model has assumed that diffusion of is independent of pixel implant geometry. There are cases when this is not a good assumption, but it seems to be appropriate in devices such as the PIN array where the gap between pixels is fully depleted.

We have also assumed that photon arrival, carrier diffusion and capture are uncorrelated. Known correlation mechanisms in photon arrival (such as Bose-Einstein or Hanbury-Brown-Twiss) and diffusion (such as carrier-carrier interaction) seem unlikely to be significant here at visible or near infrared wavelengths. If any stochastic

gain is present in the detector however, the carriers produced by a single arrival can create correlation in neighboring pixels if they diffuse to different pixels.

## VIII. CONCLUSION

In certain kinds of detector arrays, notably P-I-N and other fully-depleted devices, inter-pixel capacitive coupling can attenuate Poisson noise and cause conversion factor to be overestimated. Measuring the energy in the central autocorrelation terms is an effective and simple technique that can characterize and compensate for this effect. Inter-pixel coupling has been observed in both hybridized silicon P-I-N and hybridized indium antimonide arrays. The error in silicon P-I-N arrays was an overestimation of roughly 30 percent. It has been shown to yield more accurate modeling in P-I-N edge spread analysis. Inter-pixel coupling is a deterministic scattering mechanism, and does not reduce device DQE — whereas carrier diffusion does. As detector arrays become more sensitive, it is expected that the effects of inter-pixel capacitance will become more significant.

### Acknowledgments

We would like to thank NASA for supporting this work through various NASA grants supporting the P-I-N array research, and acknowledge NYSTAR and the New York State Center for Advanced Technology (Center for Electronic Imaging Systems) for additional support. The University of Rochester NIR lab provided the InSb data.

---

\* Electronic address: [andrew.moore@rochester.edu](mailto:andrew.moore@rochester.edu); URL: <http://astro.pas.rochester.edu/~drew>

† Electronic address: [ninkov@cis.rit.edu](mailto:ninkov@cis.rit.edu)

‡ Electronic address: [forrest@astro.pas.rochester.edu](mailto:forrest@astro.pas.rochester.edu)

<sup>1</sup> S. Kavadias, K. Misiakos, and D. Loukas, “Calculation of Pixel Detector Capacitances through Three Dimensional Numerical Solution of the Laplace Equation,” *IEEE Transactions on Nuclear Science* **40** (2), pp. 397–401, April 1994.

<sup>2</sup> Caccia, M. and Borghi, S. and Campagnolo, R. and Battaglia, M. and Kucewicz, W. and Palka, H. and Zalewska, A. and Domanski, K. and Marczewski, J, “Characterisation of Hybrid Pixel Detectors with capacitive charge division,” *5th international Linear Collider Workshop*, 2001.

<sup>3</sup> Battaglia, M. and Borghi, S. and Caccia, M. and Campagnolo, R. and Kucewicz, W. and Palka, H. and Zalewska, “Hybrid Pixel Detector Development for the Linear Collider Vertex Detector,” *9th International Workshop on Vertex Detectors*, 2001.

<sup>4</sup> A. C. Moore, Z. Ninkov, W. J. Forrest, C. McMurtry, G. S. Burley, and L. Avery, “Operation and test of Hybridized Silicon p-i-n Arrays using Open-source Array

Control Hardware and Software,” in *Proc. SPIE, Sensors and Camera Systems for Scientific, Industrial, and Digital Photography Applications IV*, M. M. Blouke, N. Sampat, and R. J. Motta, eds., **5017**, pp. 240–253, Jan. 2003.

<sup>5</sup> L. Mortara and A. Fowler, “Evaluations of CCD: Performance for Astronomical Use,” in *Proc. SPIE, Solid State Imagers for Astronomy*, **290**, pp. 28–33, 1981.

<sup>6</sup> J. Janesick, K. Klaasen, and T. Elliott, “CCD charge collection efficiency and the photon transfer technique,” in *Proc. SPIE, Solid State Imaging Arrays*, **570**, pp. 7–19, 1985.

<sup>7</sup> A. C. Moore, Z. Ninkov, and W. J. Forrest, “Interpixel capacitance in nondestructive focal plane arrays,” in *Proc. SPIE, Focal Plane Arrays for Space Telescopes*, T. J. Grycewicz and C. McCreight, eds., **5167**, pp. 204–217, Aug. 2003.

<sup>8</sup> J. D. Gaskill, *Linear Systems, Fourier Transforms, and Optics*, John Wiley and Sons, New York, 1978.

<sup>9</sup> J. Janesick, “Charge-coupled CMOS and hybrid detector arrays,” in *Focal Plane Arrays for Space Telescopes*, T. J. Grycewicz and C. McCreight, eds., **5167**, pp. 1–18, Aug. 2003.

<sup>10</sup> A. Piterman and Z. Ninkov, “Measurements of the sub-

- pixel sensitivity for a backside-illuminated ccd,” in *Proc. SPIE, Sensors and Camera Systems for Scientific, Industrial, and Digital Photography Applications*, M. M. Blouke and N. Sampat, eds., **3965**, pp. 289–297, 2000.
- <sup>11</sup> E. C. Doerner, “Wiener spectrum analysis of photographic granularity,” *J. Opt Soc. Am A* **52**, pp. 669–672, 1962.
- <sup>12</sup> R. Shaw, “The equivalent quantum efficiency of the photographic process,” *J. Phot. Sci.* **11**, pp. 199–204, 1963.
- <sup>13</sup> M. Rabbani, R. Shaw, and R. Van Metter, “Detective Quantum Efficiency of imaging systems with amplifying and scattering mechanisms,” *J. Opt Soc. Am A* **4** (5), pp. 895–901, May 1987.
- <sup>14</sup> M. Rabbani and R. Van Metter, “Analysis of signal and noise propagation for several imaging mechanisms,” *J. Opt Soc. Am A* **6** (8), pp. 1156–1164, Aug 1989.
- <sup>15</sup> J. Yao and I. A. Cunningham, “Parallel Cascades: New ways to describe noise transfer in medical imaging systems,” *Journal of Medical Physics* **6** (8), pp. 2020–2038, Oct 2001.
- <sup>16</sup> A. C. Moore, “Operating, Testing, and Evaluating Hybridized Silicon P-I-N Arrays.” Ph.D. dissertation, Rochester Institute of Technology Center for Imaging Science, to be published.
- <sup>17</sup> H. Holloway, “Collection Efficiency and Crosstalk in Closely Spaced Photodiode Arrays,” *Journal of Applied Physics* **60**, pp. 1091–1096, 1986.
- <sup>18</sup> B. Pain and B. Hancock, “Accurate Estimation of Conversion Gain and Quantum Efficiency in CMOS Imagers,” in *Proc. SPIE, Sensors and Camera Systems for Scientific, Industrial, and Digital Photography Applications IV*, M. M. Blouke, N. Sampat, and R. J. Motta, eds., **5017**, pp. 94–103, Jan. 2003.